Isotope effects on particle transport in Compact Helical System

K. Tanaka[1,2], S. Okamura[1], T. Minami[3], K. Ida[1,4], D.R. Mikkelsen[5], M. Osakabe[1,4], Y. Yoshimura[1], M. Isobe[1,4], S. Morita[1,4], and K. Matsuoka[1]

[1]*National Institute for Fusion Science, Toki, Gifu, 509-5292, Japan*
[2]*Kyushu University, Department of Advanced Energy Engineering, Kasuga, Fukuoka, 816-8580, Japan*
[3] *Kyoto University, Institute of Advanced Energy, Uji, Kyoto, 611-0011,Japan*
[4] *SOKENDAI (The Graduate University for Advanced Studies), Toki, Gifu, 509-5292, Japan*
[5] *Princeton Plasma Physics Laboratory, Princeton, New Jersey 08543, USA*

E-mail: ktanaka@nifs.ac.jp

The hydrogen isotope effects of particle transport were studied in hydrogen and deuterium dominant plasmas of the Compact Helical System (CHS). Longer decay time of electron density after the turning-off of the gas puffing was observed in the deuterium dominant plasma suggesting that the recycling was higher and/or the particle confinement was better in the deuterium dominant plasma. Density modulation experiments showed the quantitative difference of the particle transport coefficients. Density was scanned from $0.8\times10^{19}m^{-3}$ to $4\times10^{19}m^{-3}$ under the same magnetic field and the same heating power. In the low density regime (line averaged density $<2.5\times10^{19}m^{-3}$), the lower particle diffusivity and the larger inwardly directed core convection velocity was observed in the deuterium dominant plasma, while in the high density regime (line averaged density $>2.5\times10^{19}m^{-3}$) no clear difference was observed. This result indicates that the isotope effects of particle transport exist only in the low density regime. Comparison with neoclassical transport coefficients showed that the difference of particle transport is likely to be due to the difference of turbulence driven anomalous transport. Linear character of the ion scale turbulence was studied. The smaller linear growth rate qualitatively agreed with reduced particle transport in deuterium dominant plasma in low density regime.

1. Introduction

Hydrogen isotope effects on transport are important for predicting the performance of the future fusion reactor. In tokamak, the different characteristics of the isotope effects between hydrogen and deuterium plasmas have been reported. In tokamak, the H mode threshold power is approximately twice higher in the hydrogen plasma than in the deuterium plasma[1-4]. In JT-60U, for the same absorbed neutral beam power, the ion thermal diffusivity is approximately twice higher in the hydrogen plasma than in the deuterium plasma. As a result, the achieved stored energy in the deuterium plasma is twice that in the hydrogen plasma [5], while in helical devices isotope effects on the energy transport are less clear. In the 0.4MW ECRH heating in W7-AS, the stored energy is only 20% higher in the deuterium plasma than in the hydrogen plasma [6]. There are differences in the edge turbulence characteristics for the hydrogen and deuterium plasmas. In TEXTOR, long range correlation (LRC), which is a possible indication of the zonal flow, decreases clearly with the increase in the hydrogen content [7]. However, the small decrease in LRC with the increase in the hydrogen content is observed in TJ-II [8]. Such differences of the isotope effects in tokamak and helical devices suggest that the difference of the magnetic configuration parameters such as magnetic ripple, magnetic curvature, and magnetic shear play roles. On the other hand, there is no systematic study regarding the isotope effects on the particle transport both in tokamak

and helical devices. In this article, we report isotope effects on the particle transport for the first time. Experiments were carried out in Compact Helical System (CHS) at the National Institute for Fusion Science in 1998-1999. The data are mined and analysed for the isotope effects study. This study also aims to predict the transport characteristics of deuterium experiments planned from 2017 in the Large Helical Device (LHD). In Section 2, the difference of the decay time in the deuterium and hydrogen dominant plasma are shown. In Section 3, the results of density modulation experiments for the quantitative study of particle transports are described. In Section 4, comparison between global energy and particle confinements are shown. In Section 5, the roles of neoclassical and turbulence driven anomalous transport are discussed from the comparison with numerically calculated neoclassical particle transport coefficients and linear gyrokinetic analysis. Finally, the results are discussed and summarized in Section 6.

2. Global behaviour of particle transport in the hydrogen and deuterium plasmas

CHS is an l = 2, m = 8 heliotron/torsatron device that started operation in 1988. The major radius is 1.0 m and the averaged minor radius is 0.2 m. Plasma is produced by 53.2 GHz electron cyclotron heating (ECH) and additionally heated by the neutral beam injection (NBI) [9]. In the series of experiments, the toroidal magnetic field was 0.88T. The particle transport study was performed for the NBI heating phase. The magnetic axis position (R_{ax}) was 0.92m. At R_{ax} = 0.92m, a good performance of global energy confinement was reported due to the smaller helical ripple and a good NBI deposition compared with the other magnetic axis positions [10]. At R_{ax}=0.92m, the plasma inner boundary of the vertically elongated cross section attaches to the inner vessel wall. Thus, the recycling effects are relatively stronger compared with the outer axis configurations. The effect of the recycling should be considered in order to investigate the particle transport.

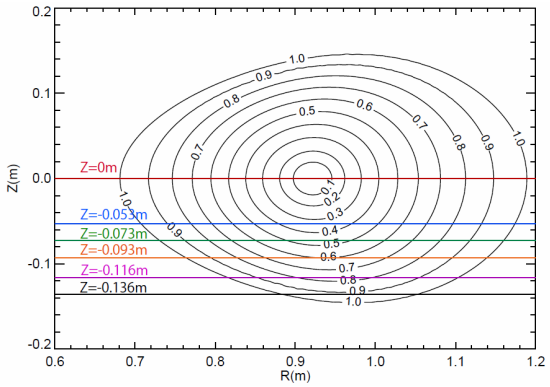

Fig. 1 Chord positions of HCN laser interferometer in CHS

First, for the study of global particle transport, the temporal evolutions of the electron density were investigated. The two-channel interferometer by using a 337μm wavelength HCN laser at the horizontally elongated cross section [11] was used for the study of the particle transport. The chord positions are shown in Fig.1. One chord passes at the plasma center (z=0), the other scans from z=- 0.053 ~ - 0.136m shot by shot. The series of scans covers almost the entire regime of the plasma.

Figure 2 shows the comparison of the time evolution for the hydrogen and deuterium dominant plasmas. After the production of plasma by using 53.2GHz ECRH, the plasma was heated by the 200kW neutral beam injection. The data set was composed of the five reproducible shots. The injected neutral beam species was hydrogen. The hydrogen and the deuterium fueling gases were switched in the series of shots. As shown in Fig. 2 (a-1) and (b-1), the decay times of density are clearly different in the hydrogen and deuterium dominant plasmas. The density decay time at the central chord of z = 0 m is 20 msec and 120 msec in the hydrogen and deuterium dominant plasmas, respectively. The difference of factor 6 was observed. However, the decay time is determined partly by the particle transport and partly by the recycling effects. Both effects are not distinguishable from these observations. The observed difference of the density decay does not prove the conclusive remarks. However, the

observed difference of the density decay time motivated us to perform further study of the particle transport. Then, gas puff modulation experiments were performed for the quantitative study.

The difference of the global energy confinement time (τ_E) is much more modest. It is only 20% longer in the deuterium dominant plasma than in the hydrogen dominant, as shown in Fig. 2 (a-2) and (b-2). The enhancement of τ_E almost disappears after the normalization by ISS95 scaling [12].

Figure 3 shows the expanded views of Fig. 2 (a-1) and (b-1). As shown in Fig. 3 (b), in the deuterium dominant plasma, sawteeth-like oscillations are excited. According to the previous study [13], this sawteeth-like oscillation is likely to be due to the fast-ion-driven instability. On the other hand, such oscillations are not visible in the hydrogen dominant plasma as shown in Fig. 3 (a). The difference of the observation of the sawteeth-like oscillation suggests that fast ion confinement is better in the deuterium dominant plasma.

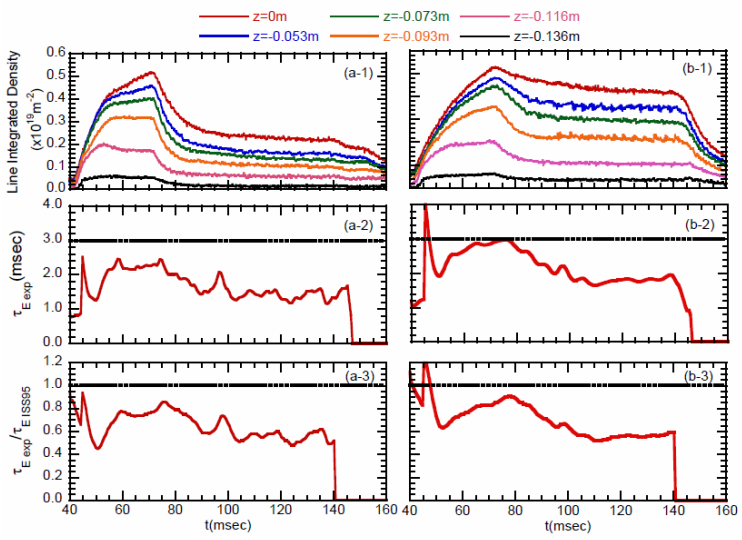

Fig. 2 Comparison of discharges in the hydrogen (a-1,2,3) and the deuterium dominant (b-1,2,3) plasmas.
(a-1) (b-1): line integrated density; (a-2) (b-2): global energy confinement time; (a-3) (b-3): H factor.
z in (a-1) and (b-1) are the vertical position of horizontally viewing interferometer chord as shown in Fig. 1. z = 0 is the chord at the plasma center, z = - 0.053, - 0.073, - 0.093, - 0.116, and - 0.136 m correspond to the tangent position of the normalized minor radius ρ=0, 0.35, 0.42, 0.49, 0.55, 0.62, 0.77, and 0.91, respectively. The line-integrated density 0.5×10^{19} m^{-2} at z = 0m, corresponds to the line-averaged density $1\times10^{19}m^{-3}$ for the path length 0.5m of the chord.

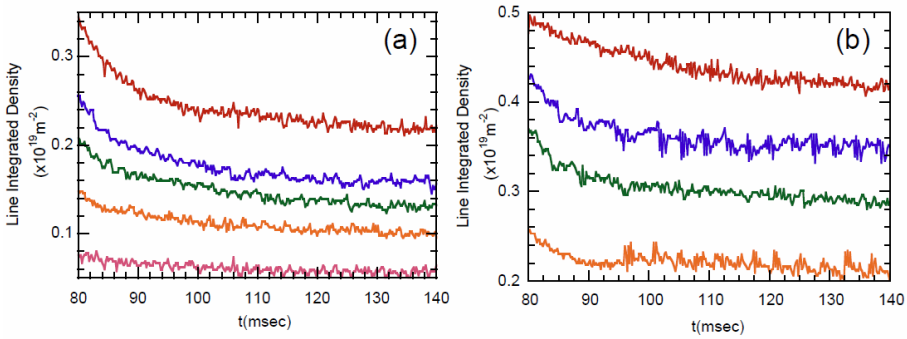

Fig. 3 Expanded view of Fig. 2 (a) hydrogen and (b) deuterium dominant plasma.

3. Quantitative analysis of particle transport in hydrogen and deuterium plasmas

3.1 Analysis procedure of density modulation experiments

For the quantitative study of particle transport, density modulation experiments were conducted. From the radial propagation of modulated density, the diffusion coefficient (D) and convection velocities (V) are separately estimated. The separate estimations of D and V are essential advantages of this technique. This is because almost all density profiles in tokamak and helical devices have a finite density gradient in the particle source-free region. This observation indicates that finite particle convections exist in this region. The separate estimation is not possible from the particle balance in the equilibrium state.

The analysis techniques used in this article are based on Gentle's method [14] using the numerical technique [15,16]. This analysis technique deduces D and V as fitting parameters. In this analysis, the absolute values of a particle source, which are technically difficult to measure, are not necessary. This analysis technique has been also applied in ASDEX [17], W7-S [18] and LHD [19].

Takenaga proposed a different analysis technique [20]. In this technique, D and V profiles are directly obtained from the spatial profiles of the modulation amplitude and phase. This technique does not require any spatial model of D and V. However, the technique is applicable only for the source-free region. Also, the results of D and V are sensitive to the gradient of measured phase and amplitude of density modulation. In the case of CHS, the measured quantity of density modulation from the interferometer is a line integrated quantity. Thus, it is not easy to obtain radial profiles from inversion procedure. Therefore, a technique based on Gentle's schema was used.

The following are particle balance equations of the modulation components in the cylindrical coordinate.

$$\Gamma = -D\nabla n_e + n_e V \tag{1}$$

$$\frac{\partial n_e}{\partial t} = -\nabla\cdot\Gamma + S = -\frac{1}{r}\frac{\partial}{\partial r} r\Gamma + S \tag{2}$$

$$n_e = n_{e\,eq} + \tilde{n}, \Gamma = \Gamma_{eq} + \tilde{\Gamma}, S = S_{eq} + \tilde{S} \tag{3}$$

$$\tilde{S} = \tilde{S}e^{i\omega t}\ , \tilde{n}_e = \tilde{n}_e e^{i\omega t}, \partial\tilde{n}_e/\partial t = i\omega\tilde{n}_e \tag{4}$$

$$\frac{\partial^2\tilde{n}_e}{\partial r^2} + \left(\frac{1}{r} + \frac{1}{D}\frac{\partial D}{\partial r} - \frac{V}{D}\right)\frac{\partial\tilde{n}_e}{\partial r} - \left(\frac{V}{rD} + \frac{1}{D}\frac{\partial V}{\partial r}\right)\tilde{n}_e - i\frac{\omega}{D}\tilde{n}_e + \frac{\tilde{S}}{D} = 0 \tag{5}$$

$$\tilde{n}_e = \tilde{n}_{eR} + i\tilde{n}_{eI} \tag{6}$$

$$\frac{\partial^2\tilde{n}_{eR}}{\partial r^2} + \left(\frac{1}{r} + \frac{1}{D}\frac{\partial D}{\partial r} - \frac{V}{D}\right)\frac{\partial\tilde{n}_{eR}}{\partial r} - \left(\frac{V}{rD} + \frac{1}{D}\frac{\partial V}{\partial r}\right)\tilde{n}_{eR} + \frac{\omega}{D}\tilde{n}_{eI} + \frac{\tilde{S}}{D} = 0 \tag{7}$$

$$\frac{\partial^2\tilde{n}_{eI}}{\partial r^2} + \left(\frac{1}{r} + \frac{1}{D}\frac{\partial D}{\partial r} - \frac{V}{D}\right)\frac{\partial\tilde{n}_{eI}}{\partial r} - \left(\frac{V}{rD} + \frac{1}{D}\frac{\partial V}{\partial r}\right)\tilde{n}_{eI} - \frac{\omega}{D}\tilde{n}_{eR} = 0 \tag{8}$$

Here, the subscript *eq* indicates equilibrium components, the tilde modulation components S particle source rate, ω modulation frequency, the subscript R real part of modulation components, and the subscript I imaginary part of modulation components.

In the particle balance equation (eq.(2)), the modulation components are treated independently of the equilibrium components. Then, the frequency ω modulation components of the particle balance equation are described by eq. (5). The modulation components are complex functions and consist of real and imaginary parts (eq. (6)). Then two equations (eq. (7) and (8)) are obtained. Here, the phase of the particle source is neglected. This can be justified since the penetration speeds of neutral hydrogen and deuterium are order of km/s, while the speed of propagation of the modulation amplitude is of the order of several or several tens m/sec.

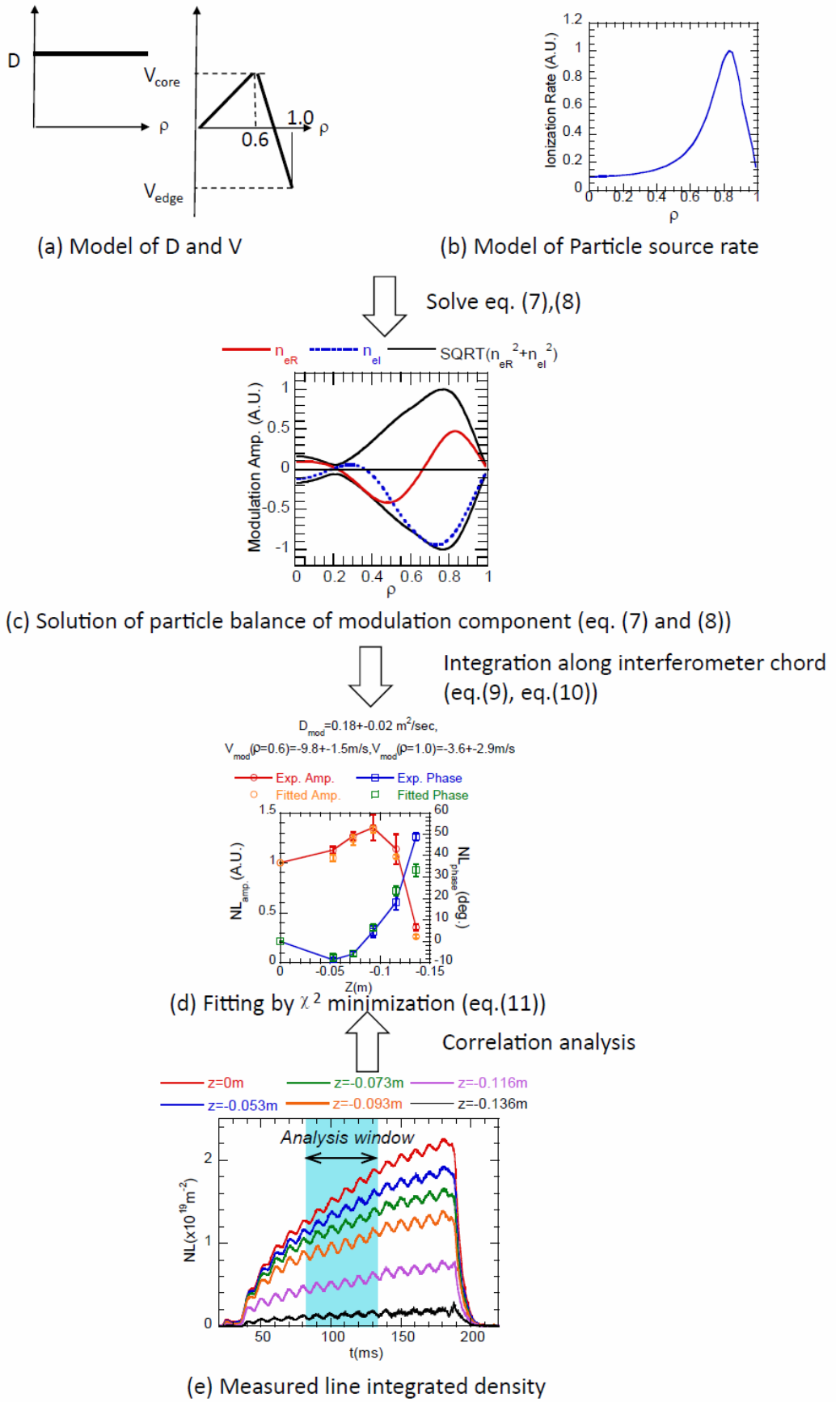

Fig. 4 Procedure to determine D and V from density modulation experiments.

In this analysis, we used the three fitting variables for D and V. One is the spatially constant D, and the other two are V at ρ = 0.6 and V at ρ = 1.0 as shown in Fig.4 (a). The convection velocity is zero at ρ = 0, then it increases linearly to V_{core} at ρ = 0.6, and then it changes linearly from V_{core} at ρ = 0.6 to V_{edge} at ρ = 1.0. The turning point of V was set to be ρ = 0.6, since the equilibrium density profile changed its gradient at around ρ = 0.6, suggesting that the particle transport changed at this location. In the series of experiments, the modulation frequency was set to be 100Hz. A frequency of 100Hz was sufficiently low in order to have a phase shift and sufficiently high in order to have several periods in the analysis time window. The particle source is also a key quantity. The profile of the particle source was taken from the analytical model of the hydrogen ionization rate, which is used in the energy balance analysis code PROCTR [21]. The penetration of the neutral hydrogen and deuterium can be different. However, according to the 3D Monte Carlo study in LHD, the difference was fairly small. Thus, the same particle source profiles were used for the analysis of both hydrogen and deuterium dominant plasmas.

Figure 4 shows the procedure of the analysis of modulation experiments to determine D and V. At first, the initial value of modeled D and V of Fig. 4 (a) and the particle source of Fig. 4 (b) are given in eqs. (7) and (8). Then, the real and imaginary parts of modulation components $\tilde{n}_{eR}$, $\tilde{n}_{eI}$ are obtained. The absolute value of the particle source is not necessary in this analysis and is an arbitrary value. With arbitrary value of particle source arbitrary values of solution eqs. (7) and (8) are obtained as shown in Fig. 4 (c). However, coefficients of eqs. (7) and (8) including D and V does not change. These solutions are integrated along the interferometer channels. Then, the integrated modulation amplitude and phase are obtained by the following equations,

$$\widetilde{NL}_{amp}(ch) = \sqrt{(\int \tilde{n}_{eR} dl\ )^2 + (\int \tilde{n}_{eI}\, dl\ )^2} \tag{9}$$

$$\widetilde{NL}_{phase}(ch) = \tan^{-1}(\int \tilde{n}_{eI}\, dl\ / \int \tilde{n}_{eR} dl\ ) \quad . \tag{10}$$

The line integrated modulation amplitude and phase, which are given by eqs. (9) and (10), are compared with the modulation amplitude and phase, which are measured by the interferometer. Finally, the iterative fitting procedure is performed to minimize the following χ^2 in order to obtain the optimized D and V. In eq. (11), the subscripts exp and calc indicate the experimental values and the calculated values, respectively. Such D and V account for the experimental observations as shown in Fig. 4 (d).

$$\chi^2 = \Sigma_{ch}\left\{\left(\int \tilde{n}_{eRexp} dl - \int \tilde{n}_{eRcalc}\, dl\ \right)^2 + \left(\int \tilde{n}_{eIexp} dl - \int \tilde{n}_{eIcalc}\, dl\right)^2\right\} \tag{11}$$

$$\int \tilde{n}_{eRexp} dl = \widetilde{NL}_{amp} \cos\left(\widetilde{NL}_{phase}\right) \tag{12}$$

$$\int \tilde{n}_{eIexp} dl = \widetilde{NL}_{amp} \sin\left(\widetilde{NL}_{phase}\right) \tag{13}$$

Figure 4 (e) shows examples of the line integrated density measured by the interferometer. Figure 4 (e) consists of five reproducible shots. The analysis windows are 40-100msec, which covers 4 – 10 modulation periods. The time window is determined in order to keep density approximately within +-20% of the averaged values of the analysis time window. These analysis windows are sufficiently long in order to determine the modulation amplitude and the phase by the correlation analysis.

Figure 4 (d) shows an example of the fitting. The measured line integrated amplitude and phase agree with the calculated ones with D_{mod}=0.19+-0.02 m^2/sec, V_{mod} (ρ=0.6)=-9.8+-1.5m/s, and V_{mod} (ρ=1.0)=-3.6+-2.9m/s. The error of D_{mod} and V_{mod} comes from the error of the experimentally measured amplitude and phase from the correlation analysis between interferometer chords. The experimental error was defined as the variation of the phase and amplitude within the frequency peak at correlation spectrum. For the χ^2 fitting, these errors were added as a standard deviation of Gausian distribution. This error sensitivy study was repeated 100 times. Then, the

100 sets of D_{mod} and V_{mod} were obtained. Finally, the standard deviation of D_{mod} and V_{mod} of 100 times error trial were defined as error of D_{mod} and V_{mod}. This fitting technique is the same one as used in LHD modulation experiment analysis [22].

The subscript "mod" is added to D and V in order to distinguish equilibrium values. The coefficients D and V from the modulation experments can be different from D and V in the equilibrium state [23]. In the analysis of LHD [19,22], D and V are determined to fit both modulation and background equilibrium profiles simultaneously. The calculation in LHD is based on the assumption that D and V from modulation and equilibrium agree with each other. But in the analysis of CHS, fitting was done only for modulation components. This is because in CHS particle fueling from NBI is not negligible particularly in the low density regime, and the beam fueling affects the density profile in addition to transport effects. On the other hand, the particle fueling from the beam is fairly small in LHD and the density profile of equilibrium is determined by the transport only.

3.2 Comparison of the particle transport in the hydrogen and deuterium dominant plasmas

Figure 5 shows the temporal evolutions of the central line-averaged-density in the modulation experiments. By changing the external fueling rate, low (0.8-2x$10^{19}$$m^{-3}$) and high (2-4x$10^{19}$$m^{-3}$) density shots were obtained in the hydrogen and deuterium dominant plasmas. The same density regime was tried. However, in the deuterium

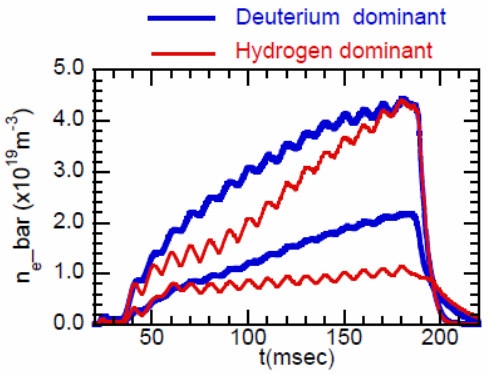

Fig. 5 Time trace of central line-averaged-density in the modulation experiments. From two series of experiments, four cases of different density regimes were analyzed for the hydrogen and deuterium dominant plasmas.

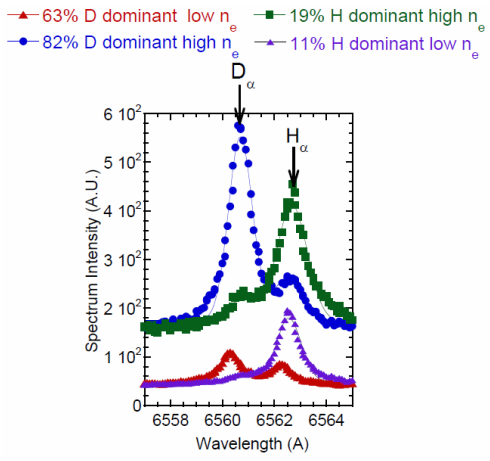

Fig. 6 Comparison of Hα and Dα spectra

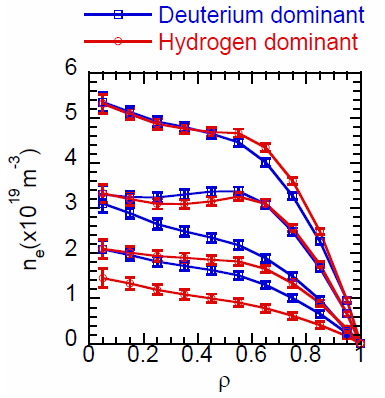

Fig. 7 Density profiles in the deuterium and hydrogen dominant plasmas

dominant plasmas, density did not reduce less than $1x10^{19}m^{-3}$. This result suggests that the recycling is higher and/or particle confinement is better in the deuterium dominant plasma. This result is also similar to the observations in Fig. 1. Experiments were carried out for the two series for both hydrogen and deuterium dominant plasmas. The analysis was performed for the different time windows of the different averaged density. In total, four different density cases were obtained both for the hydrogen and the deuterium dominant plasmas.

The fueling ratio $n_D/(n_H+n_D)x100$ (%) between hydrogen and deuterium is a key parameter for this experiment. Figure 6 shows spectra of around Hα and Dα. Fueling ratio was estimated from the intensity ratio of Hα and Dα. In the low density shot ($0.8\text{-}2.5x10^{19}m^{-3}$), the fueling ratio was 11% in the hydrogen dominant plasma and 63% in the deuterium dominant plasma. In the high density shot ($2.5\text{-}4x10^{19}m^{-3}$), the fueling ratios were 19% and 82% in the hydrogen dominant and deuterium dominant plasmas, respectively.

Figure 8 shows density dependence of D_{mod} and V_{mod}. The horizontal error bars indicate the density regime of the analysis time window. The vertical error bars indicate the fitting error of the analysis. The difference of estimated D_{mod} and V_{mod} is seen at $n_{e\_bar}<2.5x10^{19}m^{-3}$, and almost no difference is seen at $n_{e\_bar}>2.5x10^{19}m^{-3}$. This tendency is the same as the difference of the density profiles in Fig. 7. At $n_{e\_bar}<2.5x10^{19}m^{-3}$, D_{mod} becomes clearly lower in the deuterium dominant plasma than in the hydrogen dominant plasma. The global particle confinements are approximately determined by the edge diffusion coefficients [14]. Thus, the obtained results indicate that particle transport is better in the deuterium dominant plasma at $n_{e\_bar}<2.5x10^{19}m^{-3}$.

The convection velocity at ρ=0.6 is more inwardly directed in the deuterium dominant plasma than in the hydrogen dominant plasma at $n_{e\_bar}<2.5x10^{19}m^{-3}$. On the other hand, the convection velocity at ρ=1.0 is more inwardly directed in the hydrogen dominant plasma. The analysis of modulation experiments does not take into account equilibrium profiles. However, the observed differences of $V_{mod}(\rho=0.6)$ and $V_{mod}(\rho=1.0)$ qualitatively agree with the difference of equilibrium profile at $n_{e\_bar}<2.5x10^{19}m^{-3}$, where there are steeper density gradients at ρ = 0 - 0.6 in the deuterium dominant plasma and steeper density gradients at ρ=0.6-1.0 in the hydrogen dominant plasma.

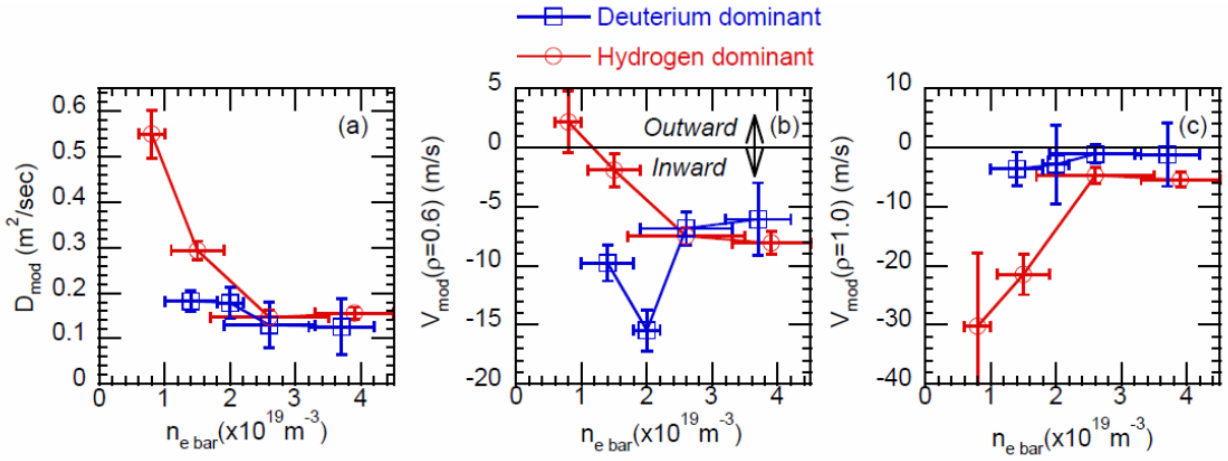

Fig. 8 Density dependence of (a) D_{mod}, (b) V(ρ=0.6), and (c) V(ρ=1.0) in hydrogen and deuterium dominant plasmas.

4. Comparison of energy transport

In this section and in the following section, transport properties are studied regarding the normalised collisionality dependences. Transport characteristics can be a function of normalised parameter, since transport scaling is often a function of such normalised parameters. In this series of experiments, the scan of the density changed the collisionality around one order of magnitude in the hydrogen dominant plasma and factor five difference in the deuterium dominant plasmas. While other normalized plasma parameters such as beta or normalized ion Larmor radius did not differ in this series of experiments very much, because Bt was fixed at 0.88T, heating power was

fixed at 500kW. Thus, collisionality is only available normalized parameter to survey. Collisionality is also important both for neoclassical and anomalous transport. Neoclassical theory shows different transport characteristics according to the collisionality. Turbulence theory tells increase of the collisionality can stabilize or destabilize turbulence depending on the modes.

We use the following normalized collisionality ν_h^* , which is defined as follows for the investigations [19].

$$\nu^*_h = \nu_{ei}/(\varepsilon_{eff}^{3/2} V_{Te}/qR) \tag{14}$$

In eq. (14), ν_{ei} is the electron ion collision frequency, V_{Te} is the electron thermal velocity, q is the safety factor and R is the major radius, ε_{eff} is an effective helical ripple. This effective helical ripple is the representative value of the magnetic ripple amplitude for multiple helicity and is defined as [24,25]:

$$\varepsilon_{eff} = \left(\frac{9\sqrt{2}}{16} \frac{\nu}{v_d^2} D \right)^{2/3} \tag{15}$$

Here, ν, v_d and D are the collision frequency, the drift velocity, and the particle diffusion coefficient in the enhanced helical ripple-trapped region, which is the so-called $1/\nu$ region, respectively. $\nu_h^*=1$ corresponds to the boundary between $1/\nu$ and plateau regime. Thus, ν_h^* is a useful normalization to find the contribution of neoclassical transport. At $\nu_h^*<1$, neoclassical contribution becomes enhanced.

Figure 9 shows ν_h^* dependence of the global energy and particle confinement time (τ_p). In Fig. 9, the global particle confinement time is defined by the following equation [26].

$$\tau_p = \frac{a^2}{5.76D} \tag{16}$$

Here, a is minor radius. D is diffusion coefficient. In eq. (16), the D_{mod} was used for D. Equation (16) is obtained by the boundary condition of the solution of the particle balance equations under the condition without particle source and diffusion coefficient is spatially constant. Contribution of convective particle transport was neglected. However, unlike decay time in Fig. 1, the recycling effects are not included and τ_p is actual particle confinement time. The following are concluded from Fig. 9. Firstly, τ_p is around factor 5-20 longer than τ_e. Generally, both τ_e and τ_p decrease with decrease of ν_h^* and at higher collisionality, τ_e and τ_p are almost similar both in deuterium and hydrogen dominant plasma. At ν_h^* ~3, τ_e is longer in hydrogen dominant plasma, while τ_p is longer in the deuterium dominant plasma. This suggests that isotope effects are different in energy and particle transport at low collisionality regime.

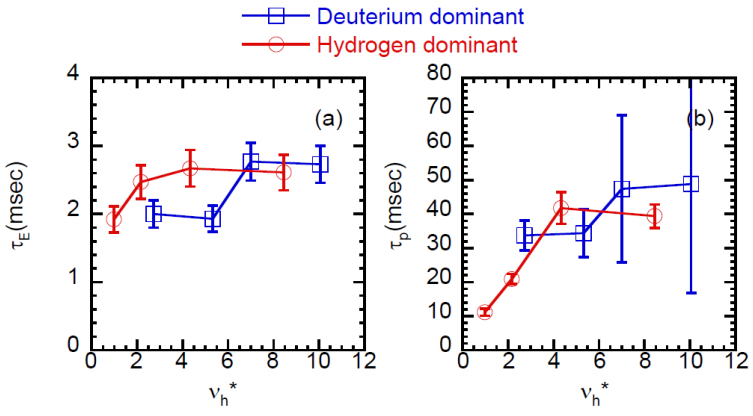

Fig. 9 Comparison of global confinement time of (a) energy and (b) particle transport.

In the series of density modulation experiments, reliable ion and electron thermal conductivities were not obtainable. This is because the spatial profiles of NBI energy deposition and the charge exchange loss of NBI were difficult to estimate at the low density regime. But, here, we make a quantitative comparison of energy transport from the profiles of density modulation experiments. Figure 10 shows comparison of n_e, T_e, and T_i profiles in the deuterium dominant and hydrogen dominant plasmas of modulation experiments. Figures 10 (a)-(c) are profiles at n_{e_bar}=1.5x10^{19}m^{-3}, and (d)-(f) are at n_{e_bar}=2.5x10^{19}m^{-3}. As shown in Fig. 9 (a), the density profile in the deuterium dominant plasma is more peaked. The differences of the T_e and T_i profiles are almost within error bars. However, there are some noticeable differences. In the low density regime (n_{e_bar}=1.5x10^{19}m^{-3}), T_e is slightly higher in the hydrogen dominant plasma while T_i is almost identical. In the high density regime (n_{e_bar}=2.5x10^{19}m^{-3}), T_e is almost identical, and T_i is slightly higher in the hydrogen dominant plasma. There is no indication of better ion and electron energy transport in the deuterium dominant plasma even in the low density regime. Higher T_e with higher n_e at low density regime in hydrogen dominant plasma (Fig.10 (a) and (b)) corresponds to the longer energy confinement time in Fig.9 (a)

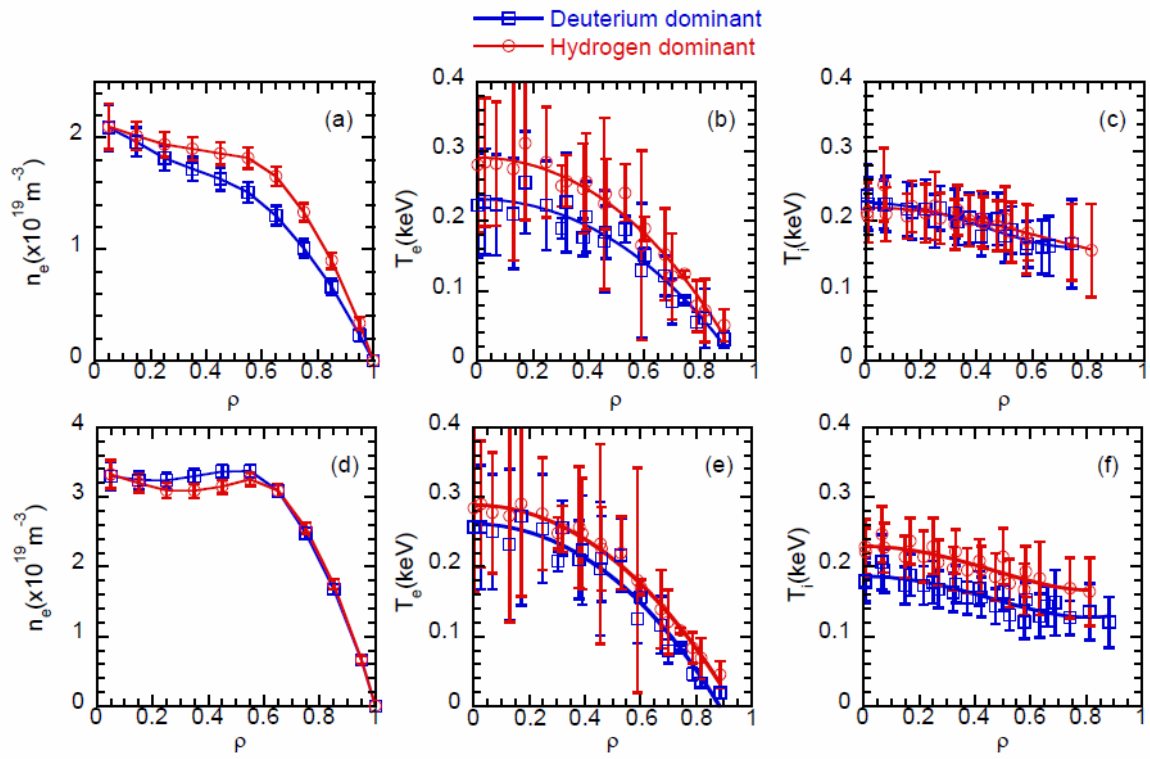

Fig. 10 Comparison of n_e, T_e, and T_i profiles in deuterium and hydrogen plasmas for (a)-(c) low density regime and (d)-(f) high density regimes of density modulation experiments. Profiles are accumulated and averaged in analysis time windows.

5. Role of neoclassical and anomalous transport

In this section, the roles of neoclassical and turbulence driven transports are investigated through comparison with numerical calculation.

5.1 Neoclassical transport

Neoclassical particle transport coefficients are calculated by GSRAKE [24] for the data set of density modulation experiments. The neoclassical particle flux is given by the following equation [27]:

$$\Gamma_{e\_neo} = -n_e D_1 \left\{ \frac{\nabla n_e}{n_e} + \frac{eE_r}{T_e} + \left(\frac{D_2}{D_1} - \frac{3}{2} \right) \frac{\nabla T_e}{T_e} \right\} \tag{17}$$

In eq. (17), D_1 is the neoclassical particle diffusion coefficient (D_{e_neo}) for electron and E_r is the neoclassical E_r field, which is self consistently determined to satisfy the ambipolarity condition by GSRAKE. The neoclassical particle convection velocity for electron was defined from the comparison between eq. (1) and eq. (17) in the following equation:

$$V_{e\_neo} = -D_1 \left\{ \frac{eE_r}{T_e} + \left(\frac{D_2}{D_1} - \frac{3}{2} \right) \frac{\nabla T_e}{T_e} \right\} \tag{18}$$

D_{e_neo} and V_{e_neo} are compared with D_{mod} and V_{mod}. In order to calculate D_{e_neo} in eq. (17) and V_{e_neo}, 100% deuterium and 100% hydrogen ions were used for the deuterium dominant and hydrogen dominant plasma respectively. However, the difference of the ion species (H+ or D+) negligibly affects electron neoclassical transport coefficients. They affect ion neoclassical transport coefficients only. Diffusion coefficients and convection velocities of deuterium ion become larger than those of hydrogen ion.

Figure 11 shows comparison of experimental and neoclassical diffusion coefficients and convection velocities in low density cases. Input profiles of neoclassical transport are shown in Figs. 10 (a) – (c). As shown in Figs.11 (a) and (c), the experimental diffusion coefficients dominates neoclassical values in almost the entire region. As shown in Figs. 11 (b) and (d), the experimental convection velocities are directed inwardly, while neoclassical ones are directed outwardly.

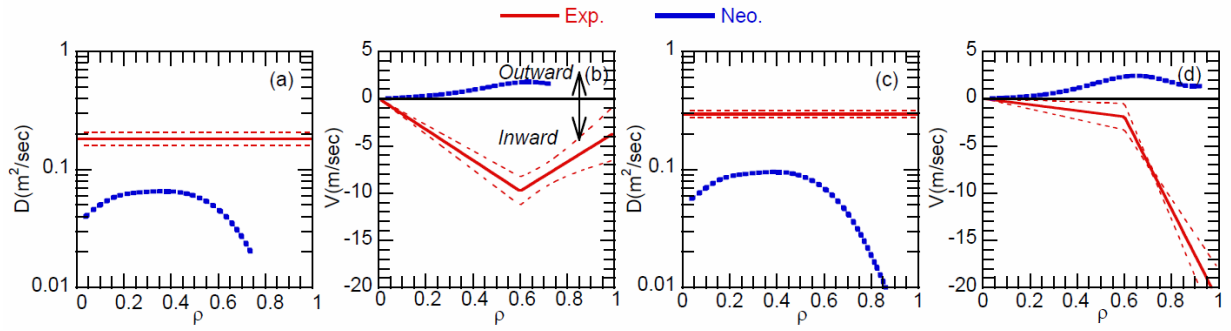

Fig. 11 Comparison of experimental D and neoclassical V (a), (b) in deuterium dominant plasma, and (c), (d) in hydrogen dominant plasma in low density case (Fig.10 (a) - (c))

Figure 12 shows ν_h^* dependence of diffusion coefficients and convection velocities of dataset of density modulation experiments. As shown in Fig. 4 (c), the peak of the modulation amplitude is at around $\rho = 0.7$, thus, the estimated D_{mod} and V_{mod} have weights around this location. Therefore, the comparisons were made at $\rho = 0.7$. As shown in Fig. 12, experimental diffusion coefficients are around one order of magnitude larger than the neoclassical values in all the data sets. Also, experimental convection velocities are directed inwardly, while neoclassical convection velocities are directed outwardly in all the data sets. These results suggest that the observed differences of the particle transport are not due to the neoclassical effects but to the turbulence driven anomalous effects.

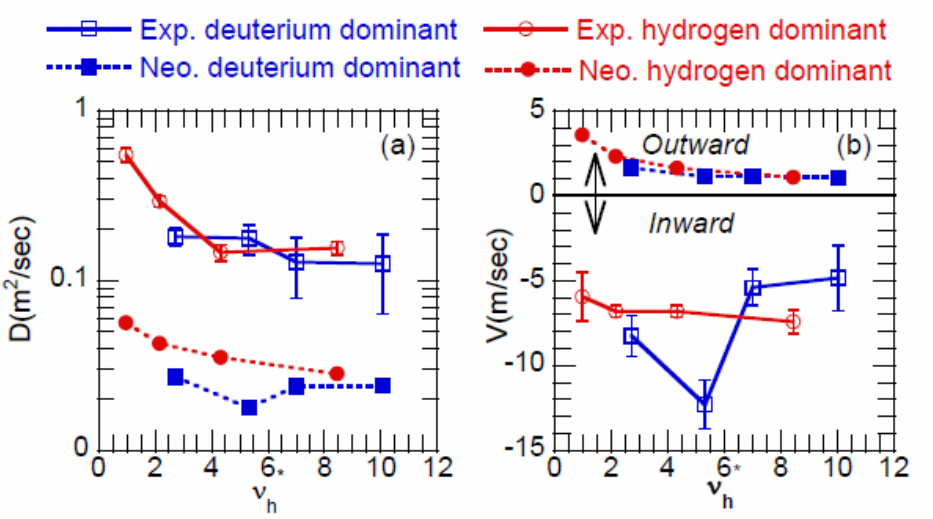

Fig. 12 ν_h^* dependence of diffusion coefficients and convection velocities of data sets of density modulation experiments. The values at $\rho = 0.7$are shown.

5.2 Turbulence driven anomalous transport

In order to investigate the role of the turbulence driven transport, linear characteristics of ion scale turbulence ($k\rho_i = 0.1\sim2$, k is the poloidal wavenumber, ρ_i is the ion Larmor radius) were studied by GS2 [28]. GS2 is a local flux tube gyrokinetic code used for linear and non-linear simulation of toroidal devices. The equilibrium of experiments of the dataset were calculated by VMEC [29], then, the magnetic properties of equilibrium were obtained by using GIST [30], and finally, grid data for GS2 were made by PPPL grid generator [31]. GS2 was benchmarked with GKV-X for ITG linear calculation in LHD [31], and quasi linear calculations of carbon particle flux were performed in LHD [32]. The linear stability analyses were performed for the kinetic motion of three charged particles, which are electron, deuterium ion, and hydrogen ions. In these analyses, collisions between charged particles were taken into account and electrostatic approximation was made.

We compared the linear spectrum and surveyed parameter dependence of linear growth rate (γ) and real frequency (ω_r). Here, for the comparison, the same unit is used for γ, ω_r, and $k\rho_i$ in the deuterium and hydrogen dominant plasma. γ and ω_r are shown in kHz and ρ_i is the hydrogen ion Larmor radius. At first, the linear spectrum was compared at $\rho = 0.7$ of low density cases (Fig. 10 (a)- (c)), where particle transports were clearly different in the deuterium and hydrogen dominant plasmas. Input data were taken from profile data (Fig. 10 (a)-(c)). Ion density ratio ($n_D/(n_D+n_H)$) was assumed to be spatially constant.

Figure 13 shows the comparison of spectrum of γ and ω_r. As shown in Fig. 13 (a), γ is higher in the hydrogen dominant plasma and an unstable region expands toward the higher $k\rho_i$. ω_r is both electron diamagnetic direction, which indicates that the most unstable turbulence mode is the trapped electron mode (TEM). ω_r is deeper in the electron diamagnetic direction in the hydrogen dominant plasma, which indicates that effects of trapped electron are larger in the hydrogen dominant plasma. Figure 14 shows eigenfunctions and variation of magnetic field strength along the field line at $\rho = 0.7$. As shown in Fig. 14, the eigenfunctions have modulations following the local helical magnetic ripple, which is shown in Fig. 14 (c). This is a typical signature of TEM in helical devices. Larger γ in hydrogen dominant plasma is qualitatively consistent with higher diffusion coefficients in the hydrogen dominant plasma.

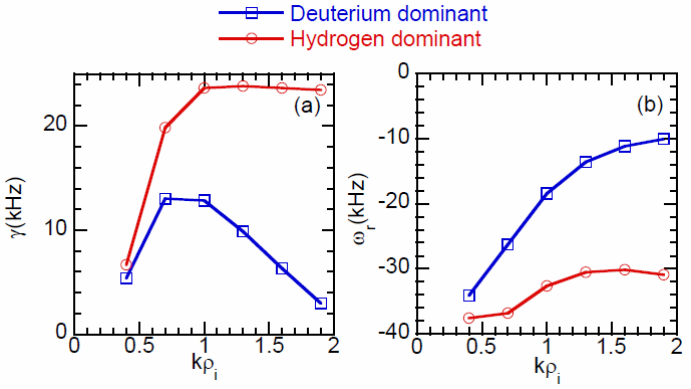

Fig. 13 Linear spectrum of (a) growth rate (γ) and (b) real frequency (ω_r). Calculated at $\rho = 0.7$ of profiles in Fig. 10 (a)-(c). The negative real frequency indicates electron diamagnetic direction in plasma frame. ρ_i is hydrogen ion Larmor radius both in the deuterium and hydrogen dominant plasma.

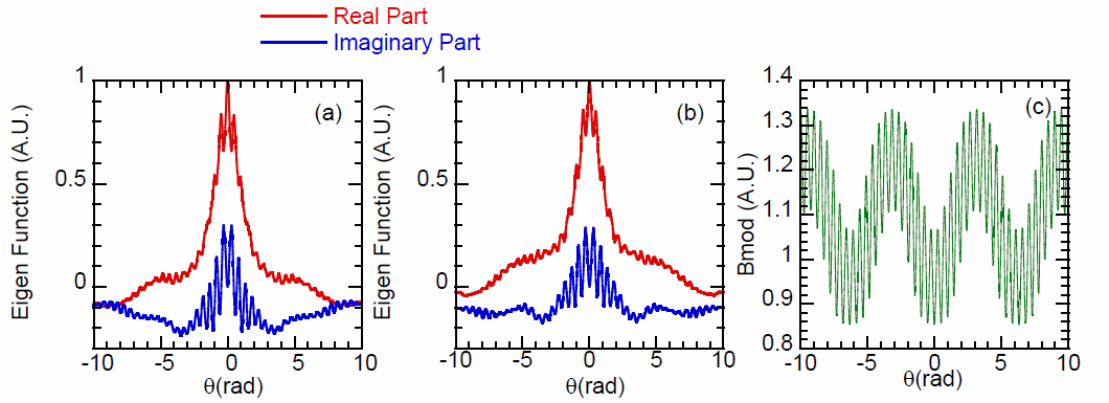

Fig. 14 Eigenfunction of $k\rho_i = 0.7$ (a) in deuterium dominant plasma, (b) in hydrogen dominant plasma and (c) magnetic field strength along the magnetic field.

Then, we investigated the parameter dependence of γ and ω_r in order to understand which parameters result in the different linear spectrum in Fig. 13. The normalized T_e gradients are almost identical both in the deuterium and hydrogen dominant plasma. The normalized T_i gradient is much smaller than the normalized T_e gradient, thus, its role is fairly small. Then, the important parameters are likely to be a ratio of deuterium and hydrogen ion ($n_D/(n_D+n_H)$), normalized density gradients (a/L_n), and collisionality. Figure 15 shows parameter dependences at $k\rho_i=0.7$, which is the peak wavenumber of γ in deuterium dominant plasma. Larger values of $k\rho_i$ will contribute little to particle transport because ion gyro-averaging diminishes the influence of small scale turbulence. In nonlinear simulations one expects an inverse cascade that transfers turbulent energy to longer scales that dominate the turbulent transport fluxes[33]. In Fig. 15 (c), the collisionality is defined as $\nu_e=\nu_{ei}\ a/\mathrm{sqrt}(2)v_{Ti}$, where ν_{ei} is electron-ion collisionality, a is minor radius and v_{Ti} is hydrogen ion thermal velocity. ν_e is an input parameter of GS2 for electron collisionality.

In order to understand parameter dependence clearly, the initial plasma parameter was fixed at the values of deuterium dominant plasma of a low density case (deuterium dominant plasma of Fig. 10 (a)-(c)). These initial settings are indicated by the plain arrow in Fig. 15. The scan region includes a parameter region, which was achieved in the density modulation experiments. Then, the parameters of the x-axis were scanned keeping other parameters constant. In Fig. 15, the x-axis values of hydrogen dominant plasma are shown by dashed arrow.

In all three parameters, γ becomes lower at values of deuterium dominant plasma. In particular, $n_D/(n_D+n_H)$ is the most influential parameter and increase of deuterium contamination results in reduction of γ. These are

favourable effects. Secondly, increase of a/L_n also reduces γ. Higher density gradient at $\rho = 0.7$ with more inwardly convection velocity helps to reduce growth rate, while ν_h^* does not show strong effect and also ν_h^* are not very different in the two cases.

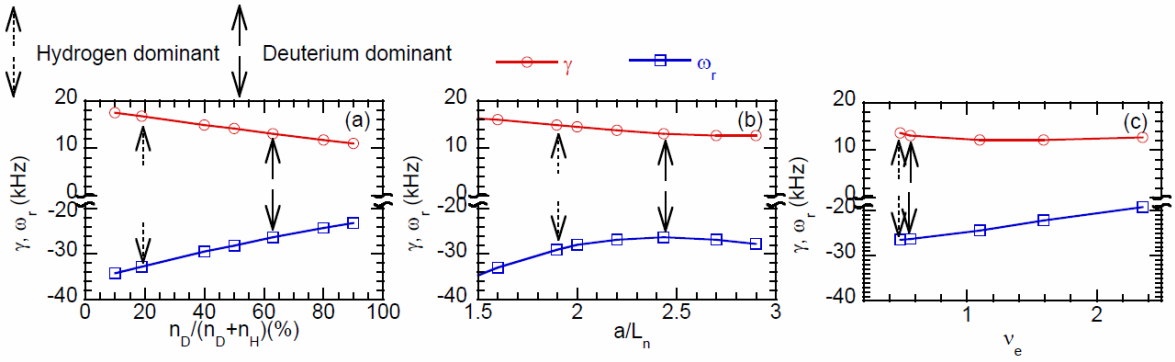

Fig. 15 Parameter dependence of linear growth rate and real frequency on (a) $n_D/(n_D+n_H)$, (b) normalized gradient $a/L_n=1/n\ dn/d\rho$ and (c) normalized collisionality ν_h^*. Plain and dotted arrow indicates value in deuterium dominant plasma low density case in Fig. 10 (a)-(c). Measured profiles of deuterium dominant plasma were used for the input parameter at plain arrow point. Then, x axis parameters were scanned keeping other input parameter. The dashed arrow indicates value at the hydrogen dominant low density plasma.

Finally, comparison of the linear characteristics of the dataset of the density modulation experiments are surveyed. Figure 16 shows γ and ω_r of $k\rho_i = 0.7$ at $\rho = 0.7$ of experimental profile of density modulation experiments. The dependences on ν_h^* are shown, however, input profiles are different at each data point. The plasma input parameters were taken from profile data of density modulation experiments. As shown in Fig. 15 (a), at lower collisionality, γ in the deuterium dominant plasma becomes smaller than those in the hydrogen dominant plasma. As shown in Fig. 15 (a) and (b), lower γ corresponds to smaller $abs(\omega_r)$ indicating that decrease of the role of trapped electrons reduces the growth rate. Comparing the experimental D_{mod} in Fig. 12 (a) and Fig. 16 (a), there is qualitative consistency, which indicates that a lower ν_h^*, D_{mod} is lower and γ is lower in the deuterium dominant plasma.

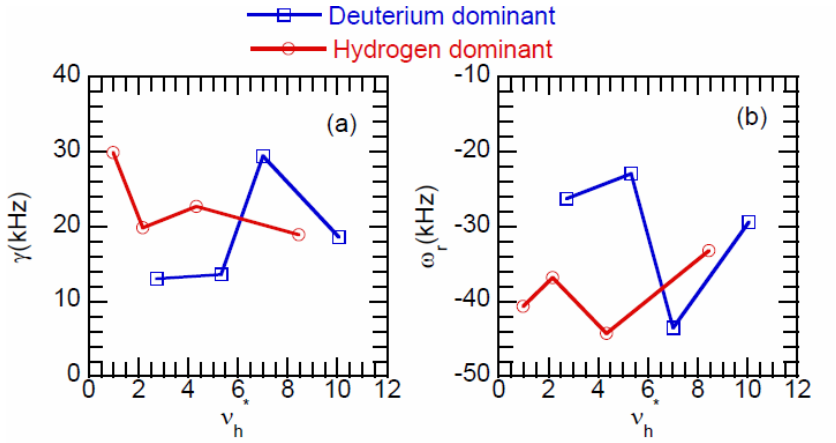

Fig. 16 (a) γ and (b) ω_r of $k\rho_i = 0.7$ at $\rho = 0.7$ of experimental profile in density modulation experiments. The profile data are from the dataset of the density modulation experiments in Sec. 3. The collisionality of each data point corresponds to the values in Fig. 12.

6. Discussion and summary

The following are concluded from the obtained results. Isotope effects of particle transport in CHS are found only in the low density regime at $n_{e\_bar}<2.5x10^{19}m^{-3}$. In this regime, D_{mod} becomes lower, V_{mod} ($\rho=0.6$) becomes more inwardly directed in the deuterium dominant plasma, and $V_{mod}(\rho=1.0)$ becomes more inwardly directed in the hydrogen dominant plasma. These changes qualitatively agree with the differences in the density decay time after turning-off of the gas puffing and in the background equilibrium profile. If the differences of D_{mod} and V_{mod} are consistent with those of D and V in equilibrium state, better particle transport and more peaked density profiles are expected in the deuterium dominant plasma in the low density regime ($n_{e\_bar}<2.5x10^{19}m^{-3}$). This will be favorable for increasing beam deposition in the central regime. The observed difference of D_{mod} at $n_{e\_bar}=1.0$-$1.8x10^{19}m^{-3}$, where data is available both in the deuterium and in the hydrogen dominant plasmas, is a factor of 1.5. This is much smaller than a factor of 6 difference of density decay time at $n_{e\_bar}=1.0x10^{19}m^{-3}$, as shown in Fig. 1. This result suggests that the longer decay time in the deuterium dominant plasma is partly determined by the higher recycling process.

In order to argue the difference of the D_{mod} and V_{mod} and D and V in equilibrium state, analyses to fit both modulation and equilibrium profiles simultaneously were also performed. This is the same analysis schema performed in LHD [19,22]. According to this analysis, the difference of D and V in the deuterium and hydrogen plasmas became smaller, while density dependence was similar. However, the fitting of modulation components became worse. The χ^2 of modulation components (eq. (11)) became a factor of 2-5 larger than the analysis with only modulation components. There are two possibilities to account for the difference of convergence between modulation only fitting and both modulation and equilibrium fitting. One is the effect of beam fueling as described in section 3.1. The other is difference of relation between normalized particle flux and normalized density gradient [23].

As shown in the following equation,

$$\begin{aligned} \delta\Gamma &= \frac{\partial\Gamma}{\partial\nabla n_e}\delta\nabla n_e + \frac{\partial\Gamma}{\partial n_e}\delta n_e \\ &= -D_{\mathrm{mod}}\delta\nabla n_e + \delta n_e V_{\mathrm{mod}} \ . \end{aligned} \qquad (19)$$

D_{mod} and V_{mod} can be interpreted as partial derivative of modulated particle flux on the density gradient and density, respectively. In the case of the second possibility, the dependences of the particle flux on density gradient and density are different in the deuterium and hydrogen dominant plasmas. In spite of these two possibilities of interpretation, it is shown that particle transport is different in the deuterium and hydrogen dominant plasma in low density regime.

The neoclassical electron particle diffusion coefficients (D_{e_neo}) are much smaller than D_{mod}. The neoclassical electron convection velocity (V_{e_neo}) showed outward direction, while V_{mod} showed inward direction. These results suggests that the particle transport process in this dataset is governed by the turbulence driven anomalous process. However, it should be noted that D_{e_neo} and V_{e_neo} are coefficients for the equilibrium profiles. For precise comparison, neoclassical D_{mod} and V_{mod} , which are defined in eq. (19), should be estimated and compared with experimental values. Such comparisons were made in W7-AS [18].

The linear growth rate is lower in the low density regime of the deuterium dominant plasma, where D_{mod} is smaller and V_{mod} is more inwardly directed. This result qualitatively agree with the reduced transport in the deuterium dominant plasma. In the present analysis of gyrokinetic linear stability, the effects of Er and Er shear are not included. Formation of Er and Er shear can stabilize unstable mode [34], however, as mentioned in Sec. 5.1, transport process is likely to be governed by an anomalous process, thus, some turbulence effects are still essential. The gyrokinetic linear calculation does not offer conclusive remarks, but it does offer the possible suggestion of a turbulence-driven mechanism. Recent gyrokinetic linear study in LHD showed favorable collision stabilization effects of TEM. TEM is more strongly stabilized in deuterium plasma than in hydrogen plasma [35]. In the next step, nonlinear simulation will be necessary for the quantitative comparison between experiments and simulations. In tokamak, isotope mass and charge effects were studied by linear and nonlinear simulation [36]. In helical plasma, nonlinear simulation requires a huge computation time because of the complicated magnetic structure. However, this is a necessary next step. Such a survey will be useful to predict optimum plasma parameters and conditions to achieve better confinement in the deuterium plasma in LHD, W7-X and future

deuterium and tritium plasma of the helical type reactor.

It should be noted that this series of experiments are in L mode. With the strong ion heating power of neutral beam, high T_i mode is achieved by improved confinement in CHS [37] as well as in LHD [38]. In the high T_i mode, T_i gradient becomes steeper, and dominant turbulence is ITG [39,40,41,42]. In ITG dominant plasma, isotope effects can be different. Also, electron collisionality (ν_e) in the series of the experiments is very high. The normalized collisionality ν_h^* is more or less comparable in CHS and LHD. This is due to the higher ε_{eff} in eq. (14) in CHS. ν_e is about 60 times higher in the CHS density modulation experiments than ν_e in the high T_i discharge of LHD. The difference of the electron collisionality may result in different turbulence characteristics.

In helical devices, experiments of isotope effects are few. Experiments in the current working helical devices such as Heliotron J, TJ-II and HSX are highly expected. These experiments will contribute to understanding the isotope effect on transport in helical devices. And the magnetic configuration may play important roles on isotope effects on the transport. This may be the reason for the differences in the observations in helical and tokamak.

Acknowledgment

One of the authors (K. T.) would like to thank Prof. Masayuki Yokoyama for providing neoclassical calculations and Dr. Motoki Nakata for useful discussions.

References

[1] ASDEX Team 1989 *Nucl. Fusion* **29** 1959
[2] Ryter F and H-Mode Database Working Group 1996 *Nucl. Fusion* **36** 1217
[3] Lackner K *et al* 1994 *Plasma Phys. Control. Fusion* **36** B79
[4] Righi E *et al* 1999 *Nucl. Fusion* **39** 309
[5] Urano H *et al*, *Phys. Rev. Lett.* **109** 125001 (2012)
[6] Stroth U *et al, Physica Scripta* **51** 655 (1995)
[7] Xu Y, Hidalgo C *et al Phys. Rev. Lett*. **110** 265005 (2013)
[8] Lin B, Pedrosa A *et al Proceeding of 41st EPS conference on Plasma Physics, Berlin, (2014)*
[9] Okamura S *et al Nucl. Fusion* **39** 1337 (1999)
[10] Kaneko O *et al in Plasma Physics and Controlled Nuclear Fusion Research 1990 (Proc. 13th Int. Conf. Washington, DC, 1990)*, *Vol. 2, IAEA, Vienna (1991) 473-481*
[11] Tanaka K *et al Rev. Sci. Instrum.* **70** 730 (1999)
[12] Stroth U *et al Nucl. Fusion* **36** 1063 (1996)
[13] Takagi S *et al Phys. Plasmas* **11**, 1537 (2004)
[14] Gentle K *et al Plasma Phys. Control. Fusion* **29** 1077 (1987)
[15] Nagashima K, Sakasai A. *Rep. JAERI-M 92-057 JAERI*, Ibaraki, 1992
[16] Tanaka K *et al Plasma Science and Technology* **8** 65 (2006)
[17] Gentle K *et al Nucl. Fusion* **32** 217 (1992)
[18] Koponen J.P.T. *et al Nucl. Fusion* **40** 365, (2000)
[19] Tanaka K *et al Fusion Science and Technology* **58** 70-90, (2010)
[20] Takenaga H *et al Nucl. Fusion* **39** 1917,(1999)
[21] Howe H C *ORNL/TM-1521 report "Physics Model in the Toroidal Transport Code PROCTR"* (1999)
[22] Tanaka K *et al Nucl. Fusion* **46** 110 (2006)
[23] Lopes Cardozo N.J. *Plasma Phys. Control. Fusion* **37** 799 (1995)
[24] Beidler C D and Hitchon W N G , *Plasma Phys. Control. Fusion* **36** ,317, (1994)
[25] Yokoyama M *et al J. Plasma Fusion Res.* **81**, 83 (2005)
[26] Chen F F, *"Introduction to plasma physics and controlled fusion", second edition, Plenum Pres*s (1984)
[27] Tribaldos V, *et al Phys. Plasma* **8**,1229 (2001)
[28] Dorland W, Jenko F, Kotschenreuther M, and Rogers B N, *Phys. Rev. Lett.* **85**, 5579 (2000)
[29] Hirshman S P and Betancourt O, *J. Comput. Phys*. **96**, 99 (1991)
[30] Xanthopoulos P *et al Phy. Plasma*, **16**, 082303 (2009)
[31] Mikkelsen D R, Nunami M, Watanabe T.-H., Sugama H, and Tanaka K, *Phys. Plasmas*, **21**, 112305 (2014)
[32] Mikkelsen D R, Tanaka K *et al Phys. Plasmas* **21**, 082302 (2014)
[33] Jenko F, Dannert T and Angioni *Plasma Phys. Control. Fusion* **47** B195 (2005)
[34] Watanabe T H, Sugama H, Nunami M *Nucl. Fusion* **51** (2011) 123003
[35] Nakata M *et al submitted to Plasma Phys. Control. Fusion*
[36] Pusztai I, Candy J, and Gohil P, *Phys. Plasmas* **18** (2011) 122501

[37] Ida K *et al Nucl. Fusion* **39** 1649 (1999)
[38] Ida K *et al Phys. Plasmas* **16** 056111 (2009)
[39] Tanaka K *et al Plasma and Fusion Research* **5** S2053 (2010)
[40] Nunami M *et al Plasma and Fusion Research* **6** 1403001 (2011)
[41] Nunami M *et al Phys. Plasmas* **19**, 4, (2012) 042504-1
[42] Ishizawa A *et al Nucl. Fusion* **55** (2015) 043024